Supporting Information

Dicyano-mediated indium framework as a heterogeneous catalyst followed by CO_2 fixation in the absence of solvent and co-catalyst

Naghmeh Bayati, Saeed Dehghanpour*

Department of Inorganic Chemistry, Faculty of Chemistry, Alzahra University, P. O. Box 1993891176, Tehran, Iran

* Corresponding author.

E-mail address: Dehghanpours@alzahra.ac.ir (S. Dehghanpour).

Experimental Section

Materials and characterization methods

All chemicals were purchased from Sigma-Aldrich and Merck chemical Companies and used without further purification. The Powder X-ray diffraction (PXRD) patterns were recorded on a Seifert XRD 3003 PTS diffractometer equipped with Cu Kα1 radiation (k = 1.5406 Å). FT-IR spectra were collected on a Bruker Tensor 27 FT-IR infrared spectrophotometer over the range of 400 – 4000 cm^{-1} using the KBr pellets method. Scanning electron microscopy (SEM) images were observed on a Philips XL-30ESEM equipped with an X-ray energy dispersive detector. Thermo gravimetric analysis (TGA) was performed using a Mettler Toledo TGA/DSC instrument with a heating rate of 10°C/min in nitrogen atmosphere. XPS (X-ray photoemission spectroscopy) results were got with a Thermo Fischer Scientific K-Alpha instrument. Elemental analyses were recorded

on a Heraeus CHN-O-Rapid elemental analyzer. TPD profiles were performed with a Micrometrics, 2750 chemisorption analyzer. Nitrogen sorption isotherms were performed using a Belsorp Mini-II instrument at 77K. Carbon dioxide sorption isotherms were recorded on a Brunauer-Emmett-Teller (BET) surface area and pore size analyzer at 298K. The catalysis products were determined by GC and G-Mass using Agilent 6890 series with a FID detector, HP-5, 5% phenylmethylsiloxane capillary, and Agilent 5973 network, mass selective detector, HP-5 MS 6989 network GC system, respectively.

Results

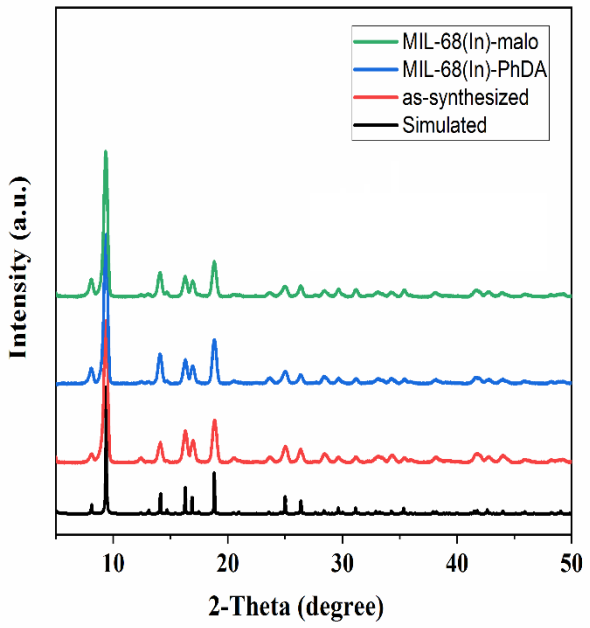

Fig. S1. Powder XRD patterns of all the synthesized catalysts.

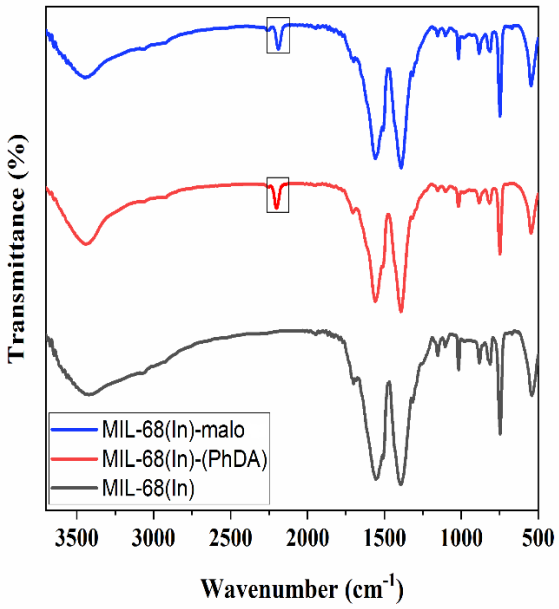

Fig. S2. FT-IR spectra of all the synthesized catalysts.

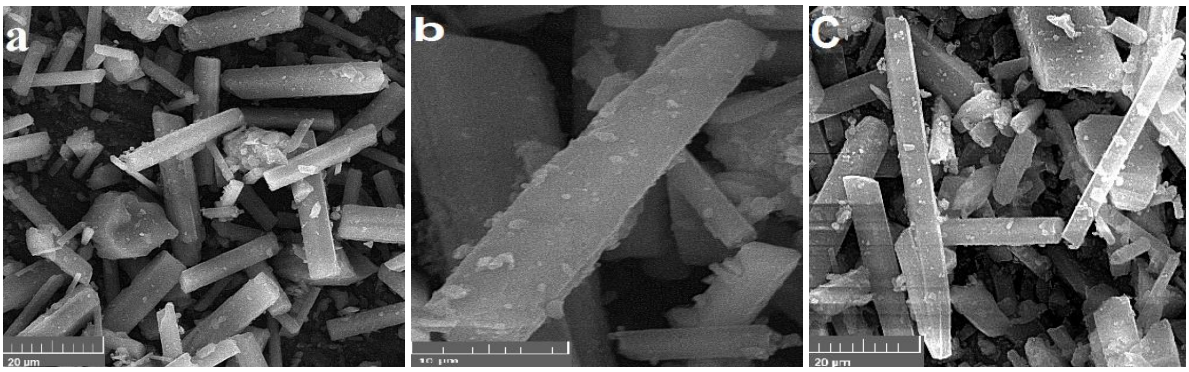

Fig. S3. SEM photographs of synthesized catalysts (a) Mil-68(In), (b) Mil-68(In)-PhDA, and (c) Mil-68(In)-malo

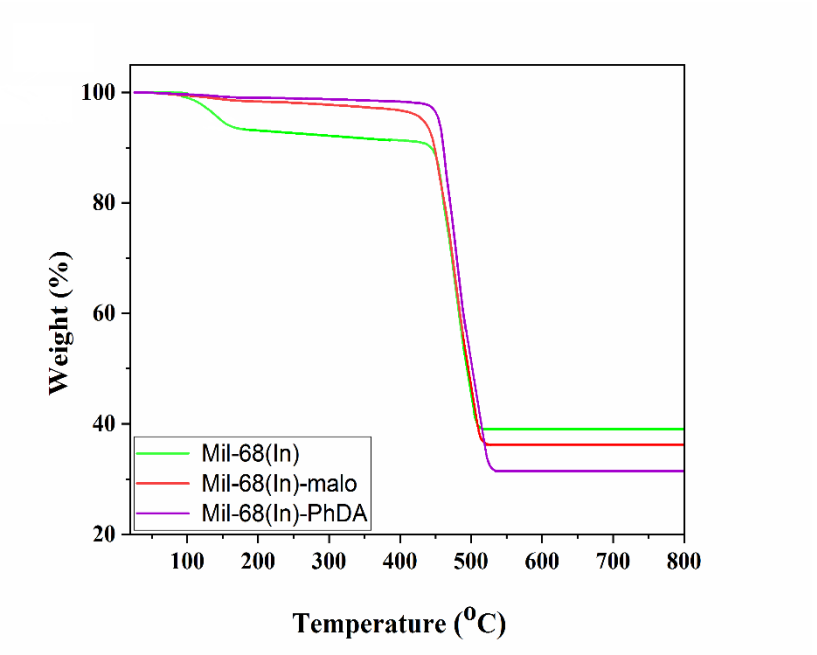

Fig. S4. TGA curves of Mil-68(In), Mil-68(In)-malo, and Mil-68(In)-PhDA

Table S1. Elemental analysis of MIL-68(In) and cyano functionalized MIL-68(In)

Entry	Catalyst	C (wt. %)	H (wt. %)	N (wt. %)	Amount of catalysts loading (wt. %)
1	MIL-68(In)-Calcd	33.37	1.32	0.76	—
2	MIL-68(In)-Found	33.34	1.30	0.75	—
3	MIL-68(In)-PhDA	36.31	2.18	4.05	22.59
4	MIL-68(In)-malo	34.52	3.29	3.77	8.89

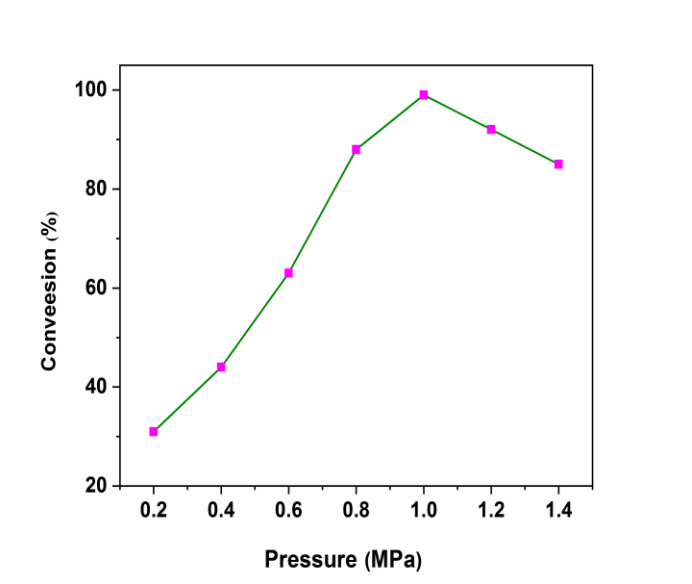

Fig. S5. Effect of CO_2 pressure on the cycloaddition of ECH over Mil-68(In)-PhDA catalyst.

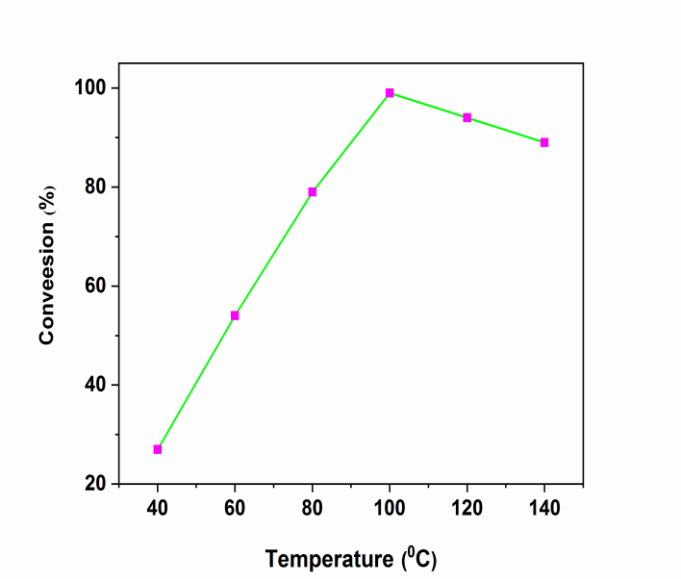

Fig. S6. Effect of temperature on the cycloaddition of ECH over Mil-68(In)-PhDA catalyst.

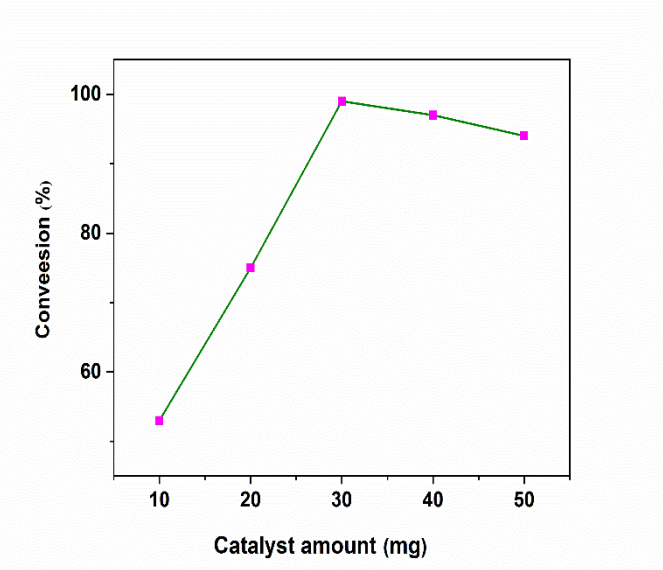

Fig. S7. Effect of catalyst amount on the cycloaddition of ECH over Mil-68(In)-PhDA catalyst.

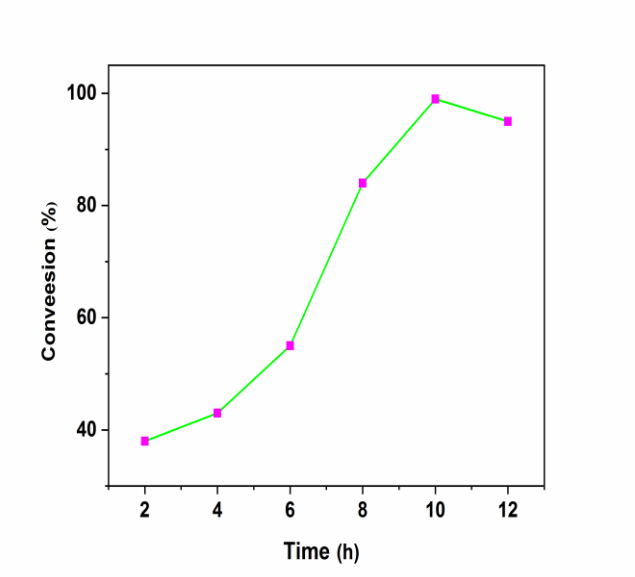

Fig. S8. Effect of reaction time on the cycloaddition of ECH over Mil-68(In)-PhDA catalyst

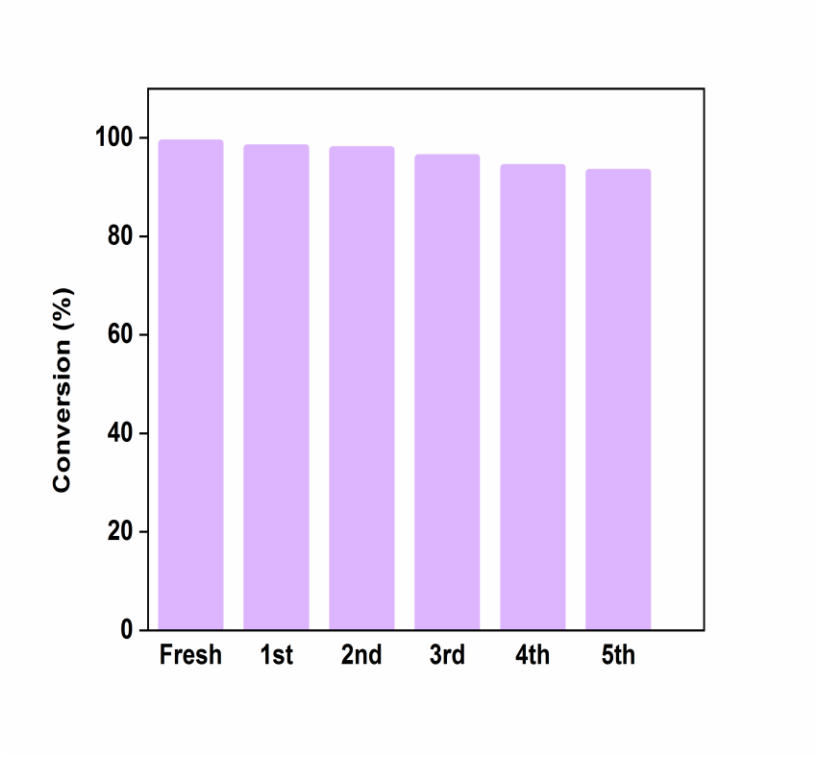

Fig. S9. Reusability test of Mil-68(In)-PhDA catalyst on the cycloaddition of ECH.

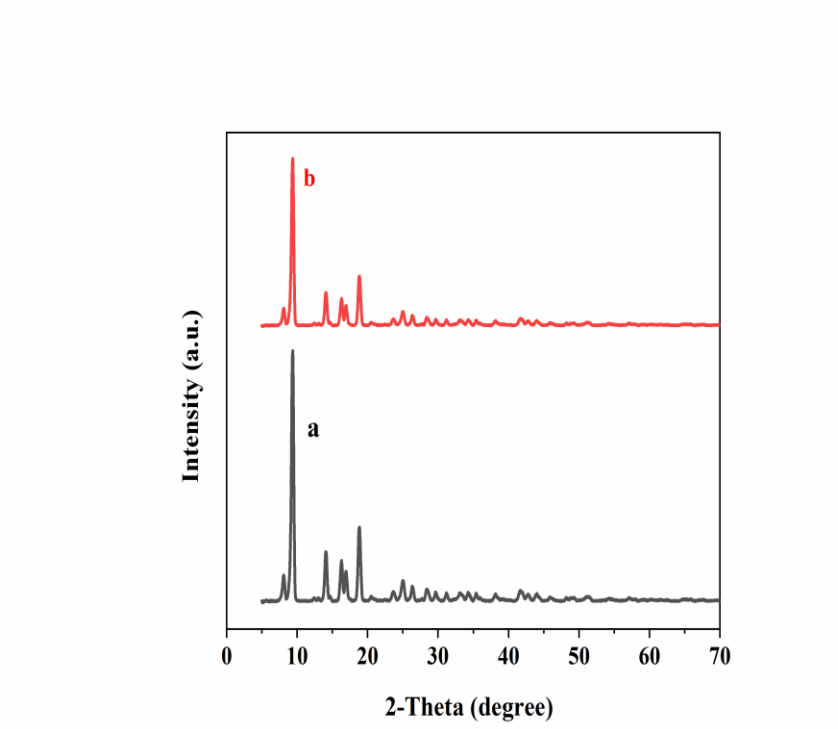

Fig. S10. XRD patterns of Mil-68(In)-PhDA (a) fresh and (b) after using 5 cycles.

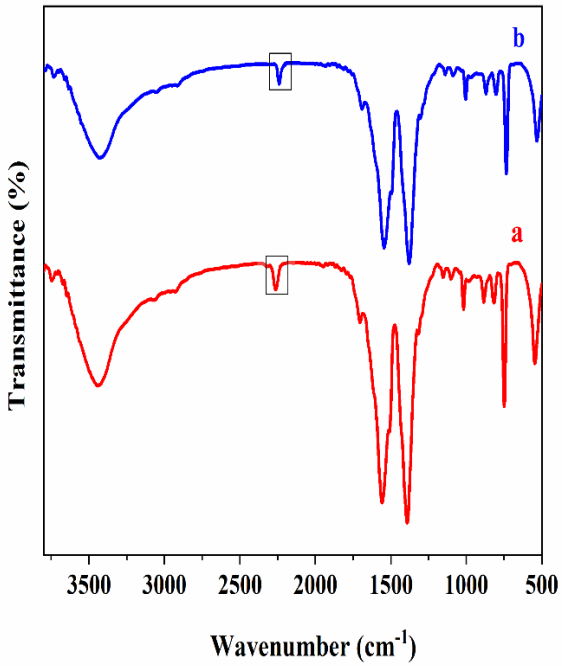

Fig. S11. FT-IR spectra of Mil-68(In)-PhDA (a) fresh and (b) after using 5 cycles.

Table S2. Textural Properties of MIL-68(In)-PhDA after catalytic cycles

Number of catalytic cycles	S BET (m2. g-1)
1	623
2	619
3	616
4	609
5	597